IJESRT

INTERNATIONAL JOURNAL OF ENGINEERING SCIENCES & RESEARCH TECHNOLOGY

Unsteady Rotating MHD Free and forced Convection Flow in a Channel

R.N Barik

Department of Mathematics, Trident Academy of Technology, Infocity, Bhubaneswar-751024, Odisha, India

barik.rabinarayan@rediffmail.com

Abstract

An analysis is made for transient, fully-developed MHD free and forced convection flow of a viscous, incompressible, Newtonian fluid in a rotating horizontal parallel-plate channel subjected to a uniform strength, static, oblique magnetic field acting at an angle to the positive direction of the axis of rotation. A constant pressure gradient is imposed along the longitudinal axis of the channel. Magnetic Reynolds number is sufficiently small to negate the effects of magnetic induction. The channel plates are electrically non-conducting. The conservation equations are formulated in an (x,y,z) coordinate system and normalized using appropriate transformations. Expressions are also derived for the primary and secondary shear stresses at the channel plates.

Keywords: MHD flow; free and forced convection flow; rotation; complex variables solutions; oblique magnetic field.

Introduction

Magnetohydrodynamic (MHD) flows with and without heat transfer, arise in numerous areas of engineering and applied physics. A prominent area of focus is MHD energy generator flows which include disk systems, solar pond hydromagnetic generators and magneto-thermo-acoustic generators. Other applications arise in hypersonic ionized boundary layers, particle deposition in electrically-conducting systems and liquid metal processing.

In numerous hydromagnetic flows, rotation may also take place and the centrifugal forces can exert a significant effect on flow dynamics and heat transfer processes. Elco et al. [1] studied analytically the characteristics of rotating flow in the radial vortex magneto-gas dynamic generator system. Further interesting studies of transient rotating hydromagnetic flow were reported by Katsurai [2] and Oliver [3].

A number of mathematical and numerical studies of transient and rotating hydromagnetic flows have also appeared, employing a wide spectrum of analytical and computational methods. For example, oscillatory hydromagnetic flow in a continuous electrode Faraday generator was studied by Ibáñez et al. [4], who also considered optimization aspects and derived generator efficiencies. Takhar et al. [5] studied unsteady hydromagnetic flow of a dusty viscous liquid in a rotating channel with Hall currents and heat transfer, obtaining exact solutions and studying in detail the effect of Hartmann number and Strouhal number on the velocity evolution in the channel. Seth et al. [6] used the Laplace transform technique to investigate transient rotating hydromagnetic Couette flow in a parallel porous plate channel, with flow induced due to the impulsive movement of the one of the plates of the channel. The plates of the channel are considered porous and the magnetic field. Asymptotic behaviour of the solution was analyzed for small as well as large values of time and it was found that suction decelerates the primary as well as secondary flow where as injection and time have accelerating influence on the primary and secondary flows. Hayat et al. [7] investigated Hall current magneto-hydrodynamics in rotating oscillating flows of a non-Newtonian fluid in a porous medium. Zueco and Bég [8] used network simulation to study the transient magneto-elasto-hydrodynamic squeezing film flow between parallel rotating disks with magnetic induction effects. Ghosh and Bhattacharjee [9] reported exact solutions for combined forced and free thermal convection hydromagnetic flow in rotating parallel plate channel with perfectly conducting walls, showing that shear stresses at the walls decrease with the increase in both the inverse Ekman number and Hartmann number squared and that the heat transfer rates at both walls decrease with the increase in the Grashof (free convection) number. Rawat et al. [10] used a variational finite element scheme to numerically simulate the laminar, fully developed, transient MHD free convection heat and mass transfer of a conducting micropolar fluid between two vertical

plates containing a non-Darcy porous medium. Strong deceleration of the flow with increasing magnetic field strength was established and also an accentuation of temperatures and concentration values of the dispersing agent indentified in the regime for strong magnetic fields. Bhargava et al. [11] investigated the periodic reactive hydromagnetic free convection velocity, thermal and species diffusion boundary layers along a plate embedded in a porous medium with Soret and Dufour effects using an optimized variational finite element code. They showed that velocity is reduced with increasing magnetic parameter, whereas a rise increase in Eckert number (dissipation parameter) elevates temperature. Furthermore it was found that increasing chemical reaction parameter enhanced velocity, temperature and also concentration value, and that temperature was increased considerably with decreasing Soret number and simultaneous increasing Dufour number. Hayat et al. [12] studied transient rotating MHD flow of a viscoelastic fluid analytically showing that a steady asymptotic hydromagnetic solution exists for blowing and resonance. The above studies have all considered the case of a transverse magnetic field i.e. a magnetic field acting perpendicular to the principal flow direction.

The objective of the present study is to consider the influence of an oblique magnetic field on the rotating transient viscous hydromagnetic flow and free and forced convection under a forced oscillation.

Mathematical Model

Consider the transient, magneto-hydrodynamic free and forced convection flow of a viscous, incompressible electrically-conducting Newtonian fluid between parallel plates, located a distance *2L* apart, along the *z* – axis, under the action of a constant pressure gradient, in an (*x, y, z*) coordinate system. We choose a Cartesian system such that the *z*– axis is perpendicular to the plates $z = \pm L$. The x – axis is in the direction of the pressure gradient. The channel rotates with uniform angular velocity, Ω, about the *z*-axis (rotation axis) transverse to the plane of the flow (*x*–*y* plane), under a static (non-oscillating), uniform magnetic field, B_0. The inclined magnetic field, B_0, is orientated at angle θ to the positive z-axis, in the x-z plane. Therefore the angle will sweep in a clockwise fashion, a circle *only in the x-z plane*: θ will increase from 0 (when B_0 is directed along the positive vertical *z*-axis direction) to 90 degrees i.e.. $\pi/2$, (when B_0 is directed along the positive *x*-axis direction), to π (when B_0 is directed along the negative *z*-axis direction), to $3\pi/2$ (when B_0 is directed along the negative *x*-axis direction) and return to *0 degrees* orientation (when B_0 is again directed along the positive vertical *z*-axis direction). The regime is illustrated in Fig. 1 below. Both the fluid and the channel rotate in unison as a rigid body with the same constant angular velocity of rotation. Since the flow is influenced by a forced oscillation a time-varying current flow of sinusoidal nature becomes relevant to the case of a displacement current with reference to the inclined magnetic field. The channel plates are both electrically non-conducting. Magnetic Reynolds number is insufficient to invoke magnetic induction effects, and furthermore ion slip, Hall current and Alfven waves are neglected in the analysis. The plates are infinite along the *x* and *y* directions, and therefore all physical quantities with the exception of pressure will be functions of the independent spatial and temporal variables, z and *t* (time) only

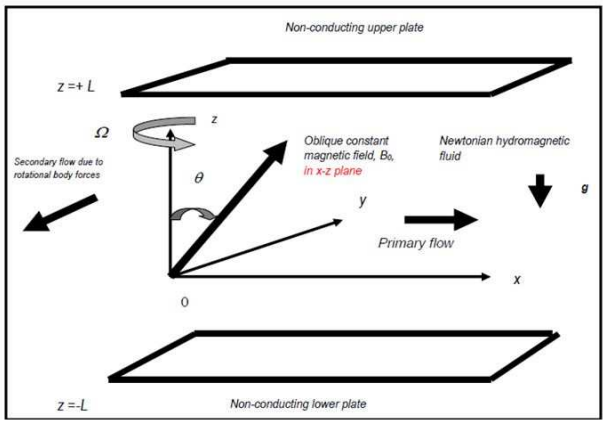

Figure 1: Physical model and coordinate system for MHD rotating channel flow.

Following Hughes and Young [13], the following vectorial field are taken

$$\boldsymbol{q} = (u',\ v',\ 0)\ ;$$
$$\boldsymbol{B} = (B'_x + B_0 \sin\theta, B'_y, B_0 \cos\theta)$$
$$\boldsymbol{E} = (E_x, E_y, E_z)\ ;$$
$$\boldsymbol{J} = (J_x, J_y, J_z) \quad (1)$$

where $\boldsymbol{q}$, $\boldsymbol{B}$, $\boldsymbol{E}$, $\boldsymbol{J}$ are respectively, the velocity vector , the applied magnetic field vector , the electric field vector and the current density vector . *u'* is the *x*–component of veloity, *v'* is the *y*– component of velocity, B'_x is the *x* – component of applied magnetic field, B'_y is the *y* – component of applied magnetic field, B_0 is the magnetic flux density and θ is the angle of inclination of the applied magnetic field with the positive direction of the axis of rotation (*z*– axis). E_x , E_y and E_z are respectively, the

components of electric field in the x, y and z directions. J_x, J_y and J_z are respectively, the x, y, z components of current densities.

The equations of motion (Navier-Stokes MHD momentum equations) under the Boussinesq approximation, for the transient magnetohydrodynamic rotating channel flow under oblique magnetic field is of the form

$$\frac{\partial \boldsymbol{q}}{\partial t}+(\boldsymbol{q}\cdot\nabla)\boldsymbol{q}+2\Omega\boldsymbol{k}\times\boldsymbol{q}=-\frac{1}{\rho}\nabla p+\nu\nabla^2\boldsymbol{q}+\frac{1}{\rho}\boldsymbol{J}\times\boldsymbol{B}$$
$$+g[1-\beta'(T-T_0)]\boldsymbol{k} \quad (2)$$

The equation of continuity (mass conservation) is:

$$\nabla\cdot\boldsymbol{q}=0 \quad (3)$$

Maxwell's electromagnetic field equations, following Hughes and Young [13], neglecting the Maxwellian displacement currents, may be stated:

$\nabla\times\boldsymbol{B}=\mu_e\boldsymbol{J}$ (Ampére's law) (4a)

$\nabla\times\boldsymbol{E}=-\frac{\partial\boldsymbol{B}}{\partial t}$ (Faraday's law) (4b)

$\nabla\cdot\boldsymbol{B}=0$. (solenoidal relation) (4c)

$\nabla\bullet\ \boldsymbol{E}=\frac{\rho}{\varepsilon_0}$ (Gauss' law) (4d)

Equations (4a-4d) effectively describe how electric charges produce electromagnetic fields. Ohm's law for a moving conductor, neglecting Hall current takes the form:

$\boldsymbol{J}=\sigma[\boldsymbol{E}+\boldsymbol{q}\times\boldsymbol{B}]$ (5)

Equation (5) effectively shows how the fields affect the charges. The following notation applies: Ω is angular velocity , ε_0 is permittivity of free space which is also known as the electric constant, t is time , g is gravity , ρ is the fluid density , ν is kinematic viscosity , μ_e is the magnetic permeability, p is pressure, σ is the fluid electrical conductivity, β is the coefficient of volume expansion, T is fluid temperature , T_0 is the temperature in the reference state , B_0 is the applied magnetic flux density (the magnetic induction, also called the magnetic field density or magnetic flux density and $\boldsymbol{k}$ is the unit vector directed along the z-axis (rotation axis). Since there is no electrical field applied in the current regime under consideration (figure 1), the polarization voltage is neglected. Therefore it follows that $\boldsymbol{E}=0$, as indicated by Meyer [14].

Under these simplifications, the governing conservations equations, in component form, may be stated as follows:

x-momentum

$$\frac{\partial u'}{\partial t}-2\Omega v'=-\frac{1}{\rho}\frac{\partial p}{\partial x}+\nu\frac{\partial^2 u'}{\partial z^2}-\frac{\sigma B_0^{\ 2}}{\rho}u'\cos^2\theta,$$

(6)

y-momentum

$$\frac{\partial v'}{\partial t}+2\Omega u'=\nu\frac{\partial^2 v'}{\partial z^2}-\frac{\sigma B_0^{\ 2}}{\rho}v'$$

(7)

z-momentum

$$0=-\frac{1}{\rho}\frac{\partial p}{\partial z}+g\{1-\beta'(T-T_0)\}+\frac{\sigma B_0^{\ 2}}{\rho}u'\sin\theta\cos\theta.$$

(8)

The appropriate boundary conditions (no-slip) at the plates are prescribed as:

$u'=v'=0$ at $z=\pm L$

(9)

where u', v' are velocity components in the x and y directions, respectively, θ is magnetic field orientation (degrees) and all other parameters have been hitherto defined. The final terms in Eqns. (6) and (8) designate the components of the Lorentzian hydromagnetic retarding force. Assuming uniform axial temperature variation along the plates of the channel, the temperature of the fluid may be written, following Mazumder [15] and Mazumder et al. [16] as:

$$(T-T_0)=Nx+\phi(z)$$

(10)

where N is constant (uniform wall temperature gradient parameter) and the other terms have been defined earlier. The equation of state is:

$$\rho=\rho_0[1-\beta'(T-T_0)]$$

(11)

Such a model while less complex than the conventional nonlinear convective heat transfer equation model, does nevertheless simulate one of the objectives of the present study (the net effect of buoyancy on momentum development in the channel). Using (11) and integrating Eqn. (8) effectively leads to:

$$p = -\rho_0 g \int [1-\beta'(T-T_0)]dz + \frac{\sigma B_0^{\,2}}{2} zu' \sin 2\theta + F(x)$$

(12)

Combining equations (10) and (12) we have:

$$\frac{\partial p}{\partial x} = -\rho g \beta' N z + \frac{d}{dx} F(x)$$

(13)

where *F(x)* is an arbitrary function. Finally using Eqn. (13), then Eqn (6) yields:

$$\frac{\partial u'}{\partial t} - 2\Omega v' = g\beta' N z - \frac{1}{\rho}\frac{d}{dx}\{F(x)\} + \nu \frac{\partial^2 u'}{\partial z^2} - \frac{\sigma B_0^{\,2}}{\rho} u' \cos^2\theta,$$

(14)

Equations (14), (7) and (8) under boundary conditions (9) constitute a two-point boundary value problem. This model can be solved in primitive variable form either numerically or with analytical tools. However to yield a more generalized understanding of the flow phenomena, it is pertinent and beneficial to introduce normalized variables.

Introduce the following non-dimensional variables:

$$\eta = \frac{z}{L}, \quad u = \left(\frac{L}{\nu\, p_x}\right) u', \quad v = \left(\frac{L}{\nu\, p_x}\right) v'$$

$$t = \frac{L^2 T}{\nu'}, \quad P_x = -\frac{L^3}{\rho \nu^2}\frac{dF}{dx}, Gr = \frac{g\beta N L^4}{\nu^2 p_x}$$

$$M^2 = B_0^{\,2} L^2 \left(\frac{\sigma}{\rho\nu}\right)^{1/2}, K^2 = \frac{\Omega L^2}{\nu}$$

(15)

where η is dimensionless *z*-coordinate, *u* and *v* are non-dimensional primary and secondary velocities, *T* is dimensionless time, P_x is non-dimensional pressure gradient in the *x'*-direction, *Gr* is Grashof number, M^2 is the Hartmann hydromagnetic number, and K^2 is the rotation parameter i.e. reciprocal of the Ekman number. Introducing the transformations (15) into Eqns. (14), (7) and (8) and boundary conditions (9), results in the following dimensionless equations and boundary conditions, with the elimination of the *z*-momentum equation:

Primary Momentum Equation

$$\frac{\partial^2 u}{\partial \eta^2} - \frac{\partial u}{\partial T} - M^2 u \cos^2\theta = -1 - Gr\eta - 2K^2 v,$$

(16)

Secondary Momentum Equation

$$\frac{\partial^2 v}{\partial \eta^2} - \frac{\partial v}{\partial T} - M^2 v = 2K^2 u.$$

(17)

Transformed Boundary Conditions

$u = v = 0$ at $\eta = \pm 1$

(18)

Analytical Solutions

Since the hydromagnetic flow is influenced by a forced oscillation, the following expressions are implemented for the velocity fields:

$$u(\eta, T) = u_0(\eta)\cos\omega T$$
$$v(\eta, T) = v_0(\eta)\cos\omega T$$

(19)

Utilizing expressions (19) the velocity distributions obtained for the primary (main) and secondary (cross) flows are, based on the method of complex variables.

This technique is one of the most powerful methods available in applied mathematics and fluid mechanics. It is concerned with complex functions which are differentiable in a given domain. In MHD we employ analytical functions with complex variables. A function *f(z)* is defined as analytic (Bég et al. [17] ,[18]) in a domain *D* if f(z) is defined and differentiable at all points of D. the function f(z) is analytic at a point z = z_0 in *D*, provided *f(z)* is analytic in a neighborhood. The necessary condition therefore for implementation of complex variables in e.g. magneto-hydrodynamic flows, is that the function f(z) must be differentiable not only at a point z_0, but throughout a specified neighborhood of that point. Such functions are also known as holomorphic in the domain *D*. Using this approach, the complex solutions can be shown to take the form:

$$u(\eta,T)=\left[\frac{\left(M^2\sin^2\theta+iG_{MK}^2\right)R_1-2P}{2iG_{MK}^2}\right]\left(1-\frac{\cosh(\alpha-i\beta)\eta}{\cosh(\alpha-i\beta)}-Gr\frac{\sinh(\alpha-i\beta)\eta}{\sinh(\alpha-i\beta)}\right)$$

$$-\left[\frac{\left(M^2\sin^2\theta-iG_{MK}^2\right)R_1-2P}{2iG_{MK}^2}\right]\left(1-\frac{\cosh(\alpha+i\beta)\eta}{\cosh(\alpha+i\beta)}-Gr\frac{\sinh(\alpha+i\beta)\eta}{\sinh(\alpha+i\beta)}\right)+R_1Gr\eta$$

(20)

$$v(\eta,T)=\left[\frac{2P\left(M^2\sin^2\theta-iG_{MK}^2\right)\left(M^4\sin^4\theta+G_{MK}^4\right)R_1}{8iK^2G_{MK}^2}\right]\left(1-\frac{\cosh(\alpha-i\beta)\eta}{\cosh(\alpha-i\beta)}-Gr\frac{\sinh(\alpha-i\beta)\eta}{\sinh(\alpha-i\beta)}\right)$$

$$-\left[\frac{2P\left(M^2\sin^2\theta+iG_{MK}^2\right)-\left(M^4\sin^4\theta+G_{MK}^4\right)R_1}{8iK^2G_{MK}^2}\right]\left(1-\frac{\cosh(\alpha+i\beta)\eta}{\cosh(\alpha+i\beta)}-Gr\frac{\sinh(\alpha+i\beta)\eta}{\sinh(\alpha+i\beta)}\right)-\frac{P}{2K^2}Gr\eta$$

(21)

Where $R_1=\frac{M^2}{(\alpha^2+\beta^2)^2}$, $P=1-\frac{M^2[M^2\cos^2\theta-\omega\tan\omega T]}{(\alpha^2+\beta^2)^2}$

$$\alpha,\beta=\frac{1}{2}\left[\left\langle\left\{\left(1+\cos^2\theta\right)M^2-2\omega\tan\omega t\right\}^2+G_{MK}^4\right\rangle^{\frac{1}{2}}\pm\left\{\left(1+\cos^2\theta\right)M^2-2\omega\tan\omega t\right\}\right]^{\frac{1}{2}}$$

$$G_{MK}^2=(16K^4-M^4\sin^4\theta-4\omega^2\tan^2\omega T-4\omega^2)^{1/2} \quad (22)$$

Special Cases

From the general solutions obtained in section 3, we may derive briefly some special cases, for physically pertinent regimes.

Case I: Oscillating Forced convection with an Oblique Magnetic Field

In the absence of buoyancy forces ($Gr \to 0$) the solutions (20) and (21) reduce to the case for pure forced magnetohydrodynamic convection.

$$u(\eta,T)=\left[\frac{\left(M^2\sin^2\theta+iG_{MK}^2\right)R_1-2P}{2iG_{MK}^2}\right]\left(1-\frac{\cosh(\alpha-i\beta)\eta}{\cosh(\alpha-i\beta)}\right)$$

$$-\left[\frac{\left(M^2\sin^2\theta-iG_{MK}^2\right)R_1-2P}{2iG_{MK}^2}\right]\left(1-\frac{\cosh(\alpha+i\beta)\eta}{\cosh(\alpha+i\beta)}\right) \quad (23a)$$

$$v(\eta,T)=\left[\frac{2P\left(M^2\sin^2\theta-iG_{MK}^2\right)\left(M^4\sin^4\theta+G_{MK}^4\right)R_1}{8iK^2G_{MK}^2}\right]\left(1-\frac{\cosh(\alpha-i\beta)\eta}{\cosh(\alpha-i\beta)}\right)$$
$$-\left[\frac{2P\left(M^2\sin^2\theta+iG_{MK}^2\right)-\left(M^4\sin^4\theta+G_{MK}^4\right)R_1}{8iK^2G_{MK}^2}\right]\left(1-\frac{\cosh(\alpha+i\beta)\eta}{\cosh(\alpha+i\beta)}\right)$$

(23b)

The expressions (22) will remain unchanged. This regime is of considerable interest in MHD generators, as elaborated in Vogin and Alemany [19].

Case II: Oscillating mixed Convection with a Transverse Magnetic Field

With $\theta \to 0$, the applied magnetic field, B_0 will become orientated along the *z*-axis i.e. at exactly 90 degrees ($\pi/2$ radians) to the *x-y* plane of flow. Clearly $\sin 0 \to 0$ and $\cos 0 \to 1$. Effectively Lorentzian hydromagnetic drag will be retained in both the primary flow velocity, and secondary flow velocity, via the P, α and β expressions which will still retain M^2 terms. Magnetic field, M^2 however will disappear from the expression, G_{MK}. The corresponding solutions for the primary and secondary flow fields, respectively, will then reduce from expressions (20) and (21) to:

$$u(\eta,T)=\left[\frac{\left(iG_{MK}^2\right)R_1-2P}{2iG_{MK}^2}\right]\left(1-\frac{\cosh(\alpha-i\beta)\eta}{\cosh(\alpha-i\beta)}-Gr\frac{\sinh(\alpha-i\beta)\eta}{\sinh(\alpha-i\beta)}\right)$$
$$-\left[\frac{\left(-iG_{MK}^2\right)R_1-2P}{2iG_{MK}^2}\right]\left(1-\frac{\cosh(\alpha+i\beta)\eta}{\cosh(\alpha+i\beta)}-Gr\frac{\sinh(\alpha+i\beta)\eta}{\sinh(\alpha+i\beta)}\right)+R_1Gr\eta$$

(24a)

$$v(\eta,T)=\left[\frac{2P\left(-iG_{MK}^2\right)\left(G_{MK}^4\right)R_1}{8iK^2G_{MK}^2}\right]\left(1-\frac{\cosh(\alpha-i\beta)\eta}{\cosh(\alpha-i\beta)}-Gr\frac{\sinh(\alpha-i\beta)\eta}{\sinh(\alpha-i\beta)}\right)$$
$$-\left[\frac{2P\left(iG_{MK}^2\right)-\left(G_{MK}^4\right)R_1}{8iK^2G_{MK}^2}\right]\left(1-\frac{\cosh(\alpha+i\beta)\eta}{\cosh(\alpha+i\beta)}-Gr\frac{\sinh(\alpha+i\beta)\eta}{\sinh(\alpha+i\beta)}\right)-\frac{P}{2K^2}Gr\eta \qquad (24b)$$

In this case, the expressions (22) will be affected and reduce to:

$$P=1-\frac{M^2[M^2-\omega\tan\omega T]}{(\alpha^2+\beta^2)^2}$$

$$\alpha,\beta=\frac{1}{2}\left[\left\langle\left\{2M^2-2\omega\tan\omega t\right\}^2+G_{MK}^4\right\rangle^{\frac{1}{2}}\pm\left(2M^2-2\omega\tan\omega t\right)\right]^{\frac{1}{2}}$$

$$G_{MK}^2=(16K^4-4\omega^2\tan^2\omega T-4\omega^2)^{1/2} \qquad (25)$$

In the expression (22) R_1 is affected, since α, β are affected. This case provides an excellent benchmark for the vast majority of studies in oscillatory hydromagnetics, which consider only a transverse magnetic field acting on the flow.

Case III: Oscillatory "Magnetic Mirror" buoyant Convection with Oblique Magnetic Field

With the angular frequency of oscillation, $\omega T \rightarrow \pi/2$, a resonant response arises corresponding to the condition, $\omega > \frac{1}{2}\cos\omega T(16K^4 - M^4 Sin^4\theta)^{1/2}$. The condition, $\omega > \frac{1}{2}\cos\omega T(16K^4 - M^4 Sin^4\theta)^{1/2}$ defines an oscillatory turbulent dynamo mechanism in a solar hydromagnetic regime if the strength of a magnetic field will be an appropriate level. A charged oscillation can take place with reference to a driving force to exhibit resonant fluorescence in the presence of an (driving frequency) excitation frequency, $\omega > 0$.

Case IV: Steady State Resonant Free Convection with an Oblique Magnetic Field

With the angular frequency of oscillation, $\omega T \rightarrow 0$, oscillation is eliminated in the regime. The regime is then "steady state". The velocity distributions in (20) and (21), can be expounded in two ways. The excitation frequency may be either $\omega < \frac{1}{2}(16K^4 - M^4 Sin^4\theta)^{1/2}$ or $\omega > \frac{1}{2}(16K^4 - M^4 Sin^4\theta)^{1/2}$. The former condition corresponds to a low frequency of oscillation in response to a solar dynamo mechanism, wherein the Lorentzian (magnetohydrodynamic) and Coriolis (rotational) forces are of the same order of magnitude. The latter conditions implies a resonant response of turbulent characteristics, and the flow regime is destabilized by a magnetic field. This latter condition therefore leads to a steady state resonance on the velocity field.

Shear Stress Distributions

The primary and secondary shear stresses at the upper and lower plates can be derived by taking the first gradients of the respective velocities at the lower (η = -1) and upper (η = +1) plates.

$$\left.\frac{du}{d\eta}\right|_{\eta\pm1} = \left[\frac{\left(M^2\sin^2\theta + iG_{MK}^2\right)R_1 - 2P}{2iG_{MK}^2}\right]\left(\mp\frac{(\alpha-i\beta)\sinh(\alpha-i\beta)}{\cosh(\alpha-i\beta)} - Gr\frac{(\alpha-i\beta)\cosh(\alpha-i\beta)}{\sinh(\alpha-i\beta)}\right)$$

$$-\left[\frac{\left(M^2\sin^2\theta - iG_{MK}^2\right)R_1 - 2P}{2iG_{MK}^2}\right]\left(\mp\frac{(\alpha+i\beta)\sinh(\alpha+i\beta)}{\cosh(\alpha+i\beta)} - Gr\frac{(\alpha+i\beta)\cosh(\alpha+i\beta)}{\sinh(\alpha+i\beta)}\right) + R_1 Gr \quad (26)$$

$$\left.\frac{dv}{d\eta}\right|_{\eta\pm1} = \left[\frac{2P\left(M^2\sin^2\theta + iG_{MK}^2\right) + \left(M^4\sin^4\theta + G_{MK}^4\right)R_1}{8iG_{MK}^2}\right]\left(\mp\frac{(\alpha-i\beta)\sinh(\alpha-i\beta)}{\cosh(\alpha-i\beta)} - Gr\frac{(\alpha-i\beta)\cosh(\alpha-i\beta)}{\sinh(\alpha-i\beta)}\right)$$

$$-\left[\frac{2P\left(M^2\sin^2\theta + iG_{MK}^2\right) - \left(M^4\sin^4\theta + G_{MK}^4\right)R_1}{8iG_{MK}^2}\right]\left(\mp\frac{(\alpha+i\beta)\sinh(\alpha+i\beta)}{\cosh(\alpha+i\beta)} - Gr\frac{(\alpha+i\beta)\cosh(\alpha+i\beta)}{\sinh(\alpha+i\beta)}\right) - \frac{P}{2K^2}Gr \quad (27)$$

Inspection of Eqns. (26) and (27) reveal that the primary (main flow) and secondary (cross flow) shear stress components vanish *neither* on the upper plate or the lower plate. Both shear stresses are functions of magnetic field (M^2), rotational parameter (K^2), angular frequency (ωT) and of course magnetic field orientation (θ). Closer inspection of the shear stress expressions indicates that in the forced convection case ($Gr \rightarrow 0$), flow reversal i.e. backflow, will not arise. Further analysis however indicates that the primary shear stress at the lower plate, i.e. $\left.\frac{du}{d\eta}\right|_{\eta=-1}$ will vanish at a critical value of the Grashof number. This criterion is defined as:

$$Gr_{cx} = -\frac{\cosh 2\alpha - \cos 2\beta}{\cosh 2\alpha + \cos 2\beta}\frac{F_5 G_{MK}^2 - F_4}{F_3 G_{MK}^2 + F_2}$$

(28)

where the functions F_1, F_2, F_3, F_4 and F_5 are defined respectively as:

$$F_1 = M^4 \sin^2\theta - 8K^4 + 2M^2\omega\cos^2\theta\tan\omega T + 2\omega^2 \quad (29a)$$

$$F_2 = F_1(\beta\sinh 2\alpha - \alpha\sin 2\beta) \quad (29b)$$

$$F_3 = M^2(\cosh 2\alpha - \cos 2\beta - \alpha\sinh 2\alpha - \beta\sin 2\beta) \quad (29c)$$

$$F_4 = F_1(\beta\sinh 2\alpha + \alpha\sin 2\beta) \quad (29d)$$

$$F_5 = M^2(\alpha\sinh 2\alpha - \beta\sin 2\beta) \quad (29e)$$

Since $\cosh 2\alpha > \cos 2\beta$ for all K^2, ωT and θ, the numerator in (28) will always be positive.

The secondary (cross flow) shear stress at the lower plate, i.e. $\left.\frac{dv}{d\eta}\right|_{\eta=-1}$ will also vanish at a *critical value* of the Grashof number. This criterion is defined as:

$$Gr_{cy} = -\frac{\cosh 2\alpha - \cos 2\beta}{\cosh 2\alpha + \cos 2\beta}\frac{2H_6G_{MK}^2 - H_5}{H_3 + 2H_4G_{MK}^2} \quad (30)$$

where the functions H_1, H_2, H_3, H_4, H_5 and H_6 are defined respectively as:

$$H_1 = 4K^4 - M^2\omega\cos^2\theta\tan\omega T - \omega^2 \quad (31a)$$

$$H_2 = M^2[M^4\sin^4\theta + G_{MK}^4] - 2H_1M^2\sin^2\theta \quad (31b)$$

$$H_3 = H_2(\beta\sinh 2\alpha - \alpha\sin 2\beta) \quad (31c)$$

$$H_4 = H_1(\cosh 2\alpha - \cos 2\beta - \alpha\sinh 2\alpha - \beta\sin 2\beta) \quad (31d)$$

$$H_5 = H_2(\alpha\sin 2\beta + \beta\sinh 2\alpha) \quad (31e)$$

$$H_6 = H_1(\alpha\sinh 2\alpha - \beta\sin 2\beta) \quad (31f)$$

Proceeding as with the lower plate, we find that at the *upper plate*, primary (main) flow reversal is initiated when:

$$Gr_{cx} = \frac{\cosh 2\alpha - \cos 2\beta}{\cosh 2\alpha + \cos 2\beta}\frac{F_5G_{MK}^2 - F_4}{F_3G_{MK}^2 + F_2} \quad (32)$$

Similarly secondary (cross) flow reversal arises at the upper plate when:

$$Gr_{cy} = \frac{\cosh 2\alpha - \cos 2\beta}{\cosh 2\alpha + \cos 2\beta}\frac{2H_6G_{MK}^2 - H_5}{H_3 + 2H_4G_{MK}^2} \quad (33)$$

The critical Grashof numbers given by expressions (32) and (33) will therefore be numerically equal to those yielded by expressions (28) and (30), for the primary flow, since the expressions emerge as being the same.

Results and Discussion

Computations are carried out for the fourth order ordinary coupled partial differential equations defined by equations (16), (17) subject to a forced oscillation given by the equations (19) based on the boundary conditions (18). This yields the *exact* solutions given in eqns. (20) and (21). The evolution of dimensionless primary and secondary velocity distributions given by the equations (20) and (21)

with the inclusion of (22) due to primary and secondary flows have been depicted graphically to show the influence of the various controlling parameters viz., M^2, K^2 , θ, Gr and ωT. A parametric study has also been undertaken for the response of the critical Grashof numbers for the primary and secondary flows (Gr_{cx}, Gr_{cy}) defined in equations (32) and (33) respectively, to θ (magnetic field inclination), M^2 (Hartmann number squared), K^2 (inverse Ekman number) and ωT (angular frequency of oscillation). These are depicted in tables 1 to 6. Additionally numerical evaluations of the dimensionless primary (u) and secondary (v) velocities have been conducted for both steady state ($\omega T = 0$) and transient ($\omega T > 0$) cases, for the effects of θ (inclination), M^2 (Hartmann number squared), K^2 (inverse Ekman number) and Gr (Grashof number). These are plotted in figures in figures 2 to 10**.** Default values for the control parameters in these graphs are taken as $K^2 = 4$; $\omega T = 0$ (steady state) or $\omega T = \pi/4$ (transient i.e. oscillatory flow).

$M^2\rightarrow$	2.0	5.0	8.0	10.0
$\theta\downarrow$	$\mathbf{Gr_{cx}}$	$\mathbf{Gr_{cx}}$	$\mathbf{Gr_{cx}}$	$\mathbf{Gr_{cx}}$
0	1.08222	1.20181	1.25510	1.26797
π/6	1.07974	1.20510	1.27004	1.29005
π/4	1.07708	1.20844	1.28810	1.318607
π/3	1.07423	1.21182	1.310601	1.35745
π/2	1.07117	1.21520	1.33969	1.41411

Table 1: Critical Grashof number for primary flow (Gr_{cx}) for $K^2 = 5$, $\omega T = \pi/4$, $\omega = 0.4$, with M^2 and θ variation.

$M^2\rightarrow$	2.0	5.0	8.0	10.0
$\theta\downarrow$	$\mathbf{Gr_{cy}}$	$\mathbf{Gr_{cy}}$	$\mathbf{Gr_{cy}}$	$\mathbf{Gr_{cy}}$
0	2.15679	2.22039	2.16832	2.10984
π/6	2.17596	2.36828	2.43820	2.43383
π/4	2.19565	2.56707	2.92311	3.13019
π/3	2.21585	2.84882	4.05982	5.77795
π/2	2.23651	3.27837	9.92299	9.50025

Table 2: Critical Grashof number for secondary flow (Gr_{cy}) for $K^2 = 5$, $\omega T = \pi/4$, $\omega = 0.4$, with M^2 and θ variation.

$K^2\rightarrow$	4.0	6.0	8.0	10.0
$\omega T\downarrow$	$\mathbf{Gr_{cx}}$	$\mathbf{Gr_{cx}}$	$\mathbf{Gr_{cx}}$	$\mathbf{Gr_{cx}}$
0	1.38988	1.25088	1.17166	1.12694
π/6	1.39747	1.25291	1.172057	1.12696
π/4	1.40331	1.25443	1.17234	1.12697
π/3	1.41406	1.25715	1.17283	1.12698
5π/12	1.44809	1.26500	1.17408	1.12693

Table 3: Critical Grashof number for primary flow (Gr_{cx}) for $M^2 = 10$, $\theta = \pi/4$, $\omega = 0.4$, with K^2 and ωT variation.

$K^2\rightarrow$	4.0	6.0	8.0	10.0
$\omega T\downarrow$	$\mathbf{Gr_{cy}}$	$\mathbf{Gr_{cy}}$	$\mathbf{Gr_{cy}}$	$\mathbf{Gr_{cy}}$
0	3.42504	2.32074	1.88616	1.67069
π/6	4.01867	2.41911	1.91810	1.68507
π/4	4.68019	2.50081	1.94296	1.69599
π/3	6.94456	2.66673	1.98932	1.71574
5π/12	7.74044	3.37511	2.14116	1.77532

Table 4: Critical Grashof number for secondary flow (Gr_{cy}) for $M^2 = 10$, $\theta = \pi/4$, $\omega = 0.4$, with K^2 and ωT variation.

$\omega T\rightarrow$	0	π/6	π/4	π/3	5π/12
$\theta\downarrow$	$\mathbf{Gr_{cx}}$	$\mathbf{Gr_{cx}}$	$\mathbf{Gr_{cx}}$	$\mathbf{Gr_{cx}}$	$\mathbf{Gr_{cx}}$
0	1.26155	1.26519	1.26797	1.27298	1.28816
π/6	1.28332	1.28714	1.29005	1.29531	1.31123
π/4	1.31147	1.31553	1.31861	1.32418	1.34107
π/3	1.34971	1.35411	1.35746	1.36350	1.38182
π/2	1.40536	1.41033	1.41411	1.42096	1.44176

Table 5: Critical Grashof number for primary flow (Gr_{cx}) for $M^2 = 10$, $K^2 = 5$, $\omega = 0.4$, with ωT and θ variation.

$\omega T\rightarrow$	0	π/6	π/4	π/3	5π/12
$\theta\downarrow$	$\mathbf{Gr_{cy}}$	$\mathbf{Gr_{cy}}$	$\mathbf{Gr_{cy}}$	$\mathbf{Gr_{cy}}$	$\mathbf{Gr_{cy}}$
0	1.97035	2.04568	2.10984	2.24462	2.90057
π/6	2.22388	2.33654	2.43383	2.64266	3.74946
π/4	2.72710	2.93904	3.13019	3.56813	6.76544
π/3	4.23919	4.98221	5.77795	8.26952	18.23172
π/2	16.62148	16.2931	9.50026	5.29162	2.08156

Table 6: Critical Grashof number for secondary flow (Gr_{cy}) for $M^2 = 10$, $K^2 = 5$, $\omega = 0.4$, with ωT and θ variation.

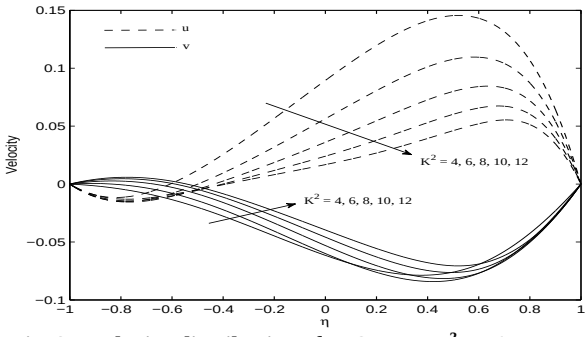

Fig. 2: Velocity distributions for $Gr = 2$, $M^2 = 10$, $\omega T = 0$, $\omega = 0.4$, $\theta = \pi/4$ for various K^2 values. (steady)

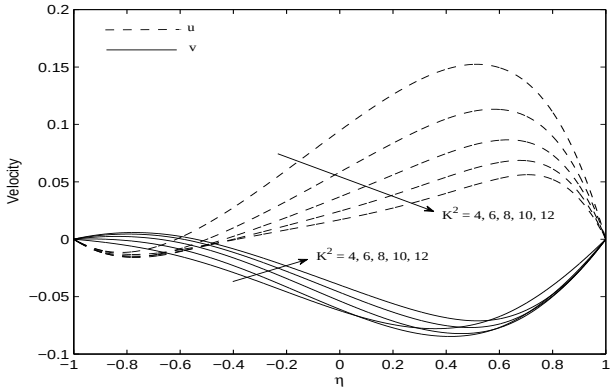

Fig. 3 Velocity distributions for $Gr = 2$, $M^2 = 10$, $\omega T = \pi/4$, $\omega = 0.4$, $\theta = \pi/4$ for various K^2 values.(transient)

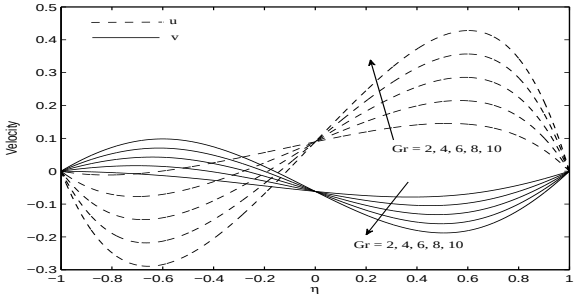

Fig. 4 Velocity distributions for $K^2 = 4$, $M^2 = 10$, $\omega T = 0$, $\omega = 0.4$, $\theta = \pi/4$ for various Gr values.(steady)

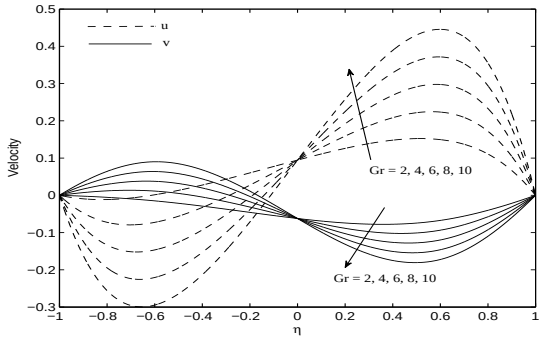

Fig. 5 Velocity distributions for $K^2 = 4$, $M^2 = 10$, $\omega T = \pi/4$, $\omega = 0.4$, $\theta = \pi/4$ for various Gr values.(transient)

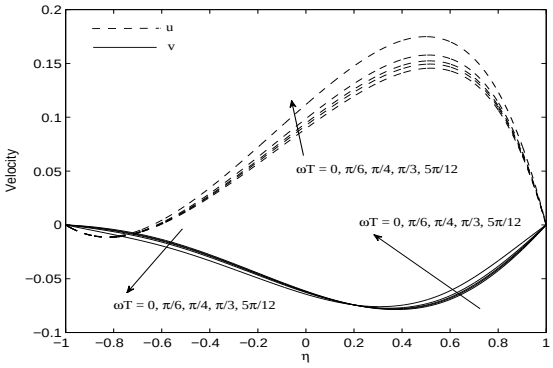

Fig. 6: Velocity distributions for $K^2 = 4$, $Gr = 2$, $M^2 = 10$, $\omega = 0.4$, $\theta = \pi/4$ for various ωT values

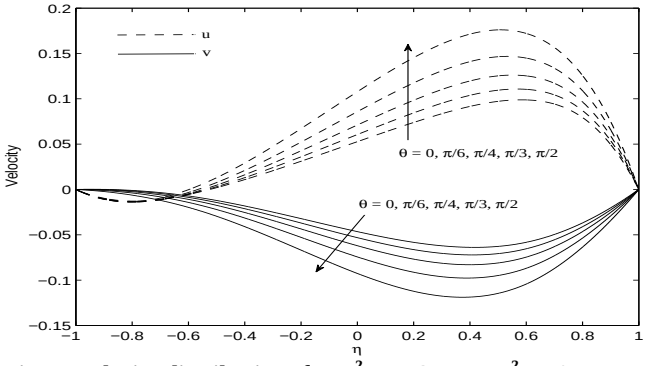

Fig. 7: Velocity distributions for $K^2 = 5$, $Gr = 2$, $M^2 = 10$, $\omega T = 0$, $\omega = 0.4$ for various θ values. (steady)

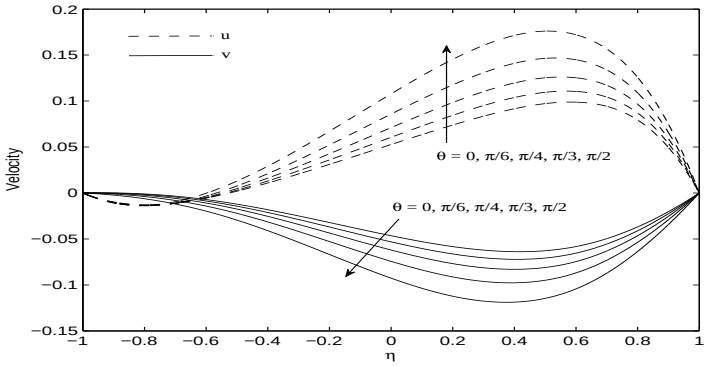

Fig. 8: Velocity distributions for $K^2 = 5$, $Gr = 2$, $M^2 = 10$, $\omega T = \pi/4$, $\omega = 0.4$ for various θ values. (transient)

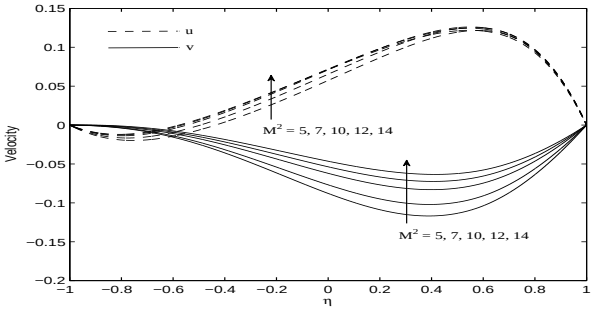

Fig. 9: Velocity distributions for $Gr = 2$, $K^2 = 5$, $\omega T = 0$, $\omega = 0.4$, $\theta = \pi/4$ for various M^2 values. (steady

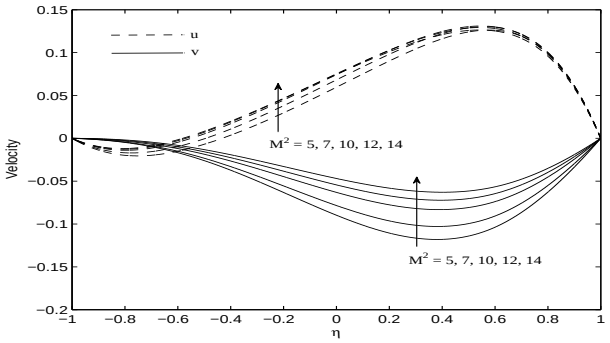

Fig. Fig.10: Velocity distributions for *Gr = 2, K² = 5, ωT = π/4, ω = 0.4, θ = π/4 for various M² values. (transient)*

Table 1 shows that Gr_{cx} remains positive for any combination of M^2 *and* θ. Positive Grashof number ($Gr_{cx} > 0$) in free convection flows implies cooling of the plate by free convection currents i.e. transport of thermal energy from the channel plates, to the intercalated fluid. We note that the opposite case, $Gr_{cx} < 0$ would correspond to plate heating, wherein free convection currents transport thermal energy from the fluid to the platesFor *any* inclination of the magnetic field, θ, Gr_{cx} magnitudes are found to increase steadily with an increase in M^2.

From Table 2 it is observed that for the variation of the critical Grashof number for the secondary flow field, i.e. Gr_{cy}. In this case we observe that at any value of M^2, Gr_{cy} is continuously boosted in magnitude with a rise in magnetic field inclination i.e. secondary critical Grashof number values progressively increase as the magnetic field sweeps from the positive *z*-axis ($\theta = 0$) through to the positive *x*-axis ($\theta = \pi/2$). Magnitudes are also found to be considerably higher than in the case of the primary critical Grashof number (Gr_{cx}), particularly at high M^2 value and greater inclinations.

In tables 3 and 4, the evolution of the primary flow and secondary flow critical Grashof numbers, i.e. Gr_{cx} and Gr_{cy}, are shown, for combinations of the rotational parameter (K^2) and the oscillation parameter (ωT). Both tables correspond to the oblique magnetic field case ($\theta = \pi/4$). Inspection of Table 3 reveals that with an increase in K^2 from 4, through
6,8 to10,at a given ωT, there is a clear decrease in Gr_{cx}. Increasing K^2 corresponds to a rise in the rotational velocity of the channel, for fixed *L* and ν ($K^2 = \frac{\Omega L^2}{\nu}$). Coriolis force is therefore boosted as K^2 is increased and this serves to reduce critical primary Grashof number magnitudes. Conversely for a fixed K^2, as the parameter ωT *increases* from 0 (transverse field case) through $\pi/6$, $\pi/4$, $\pi/3$ to the maximum inclination of $\pi/2$, *there is a steady rise in value of* Gr_{cx}. *Since* $\omega = 0.4$, *an increase in* ωT *implies that time (T) is increasing.* Hence with *progression of time,* the critical primary Grashof number is enhanced. Table 4 shows that critical Grashof number for the secondary flow (Gr_{cy}) exhibits a similar response to K^2 and ωT *i.e. with increasing* K^2 *values,* Gr_{cy} *magnitudes are depressed, and with increasing* ωT *values, magnitudes are increased*. However the values of Gr_{cy} are much higher than Gr_{cx} indicating that the secondary flow response is much stronger.

Tables 5 and 6 show the combined effects of ωT and θ *on* Gr_{cx} and Gr_{cy}. Gr_{cx} as seen in Table 5, again increases with an increase in ωT, for any value of magnetic field inclination (θ). However with greater θ, the magnitudes of Gr_{cx} are clearly enhanced. Maximum Gr_{cx} arises therefore for the maximum studied value *of* ωT *(=* $5\pi/12$*)* and the maximum value of θ *(=* $\pi/2$*)* , and attains a value of 1.44176. A similar trend is observed for the Gr_{cy} values in Table 6. However Gr_{cy} values generally increase with increasing ωT for θ = 0, π/6 and π/4; however as θ is further increased to π/3 and π/2, Gr_{cy} values rise as ωT increases to π/3 but then fall considerably for ωT = π/2.

Figures 2 to 10 show the primary (*u*) and secondary (*v*) velocity distributions across the channel for various values of the governing parameters (M^2, K^2, θ, *Gr*) for steady state ($\omega T = 0$) and transient ($\omega T = \pi/4$) cases, respectively.

Figures 2 and 3 show the effect of the rotational parameter (K^2) on *u* and *v* distributions. In the steady state case (figure 2) with increasing K^2 primary velocity is generally reduced in magnitude. *u* values are negative near the lower plate of the channel (η = -1); however for the majority of the channel space values are positive so that back flow does not arise here. Peak primary velocity arises near to the upper plate and with increasing Coriolis force (i.e. greater K^2), the peaks are displaced further from the upper plate (η = 1). Conversely the secondary flow is found to be positive near the lower plate but strongly negative everywhere else in the channel indicating that there is strong secondary flow reversal. With increasing K^2 values, *v* values are increased i.e. become more positive. A similar response is observed in figure 3 for the transient case ($\omega T = \pi/4$).

Figures 4 and 5 depict the primary and secondary velocity response to various Grashof numbers. It is observed for the steady state (figure 4) and transient (figure 5) cases. With increasing *Gr* values, primary velocity is decelerated in the lower

channel half ($-1 < \eta < 0$) whereas it is strongly accelerated in the upper channel half ($0 < \eta < 1$). Conversely secondary velocity is found to be strongly accelerated in the lower channel half ($-1 < \eta < 0$) but decelerated in the upper channel half ($0 < \eta < 1$) with an increase in Gr.

Figure 6 shows the influence of the oscillatory parameter (ωT) on the primary and secondary velocity profiles through the channel. With increasing ωT values, there is a distinct acceleration in the primary flow. Conversely the secondary flow is initially decelerated with increasing ωT values from the lower channel towards the channel mid-point, thereafter the secondary velocity is slightly accelerated with increasing ωT i.e. values become less negative. Generally the secondary velocities are negative i.e. strong secondary back flow occurs throughout the channel for all ωT.

The effects of magnetic field inclination, θ, *on* primary (u) and secondary (v) velocity profiles in the channel are shown in figures 7 and 8, for the steady state and transient cases. It is observed that a rise in inclination accelerates the primary flow (since hydromagnetic drag is reduced) and increase backflow in the secondary flow.

Finally in figures 9 and 10, we observe that for both steady state and transient cases, with an increase in the hydromagnetic parameter (M^2), primary velocity magnitudes are decreased in magnitude in the proximity of the lower plate (where back flow arises) but increased in the remainder of the channel where as secondary flow velocity magnitudes are strongly decreased throughout the channel.

Conclusions

Analytical solutions have been obtained for the transient magneto-hydrodynamic free convection flow in a rotating parallel plate channel in the presence of an inclined magnetic field. Critical Grashod numbers have been derived for the primary (main) flow and the secondary (cross) flow.

- For *any* inclination of the magnetic field, θ, Gr_{cx} *and* Gr_{cy} *magnitudes* are found to *increase steadily* with an increase in magnetic field parameter (M^2).
- Gr_{cx} *and* Gr_{cy} are increased with a rise in magnetic field inclination (θ).
- Gr_{cy} magnitudes are found to be substantially greater than Gr_{cx}, magnitudes, in particular at high M^2 value and greater inclination (θ).
- With an increase in rotational parameter (K^2), Gr_{cx} and Gr_{cy} are generally decreased.
- With increasing oscillatory parameter values (ωT) Gr_{cx} and Gr_{cy} *magnitudes are increased*.
- With increasing rotational parameter (K^2) primary velocity (u) is decreased whereassecondary velocity (v) is enhanced.
- With increasing free convection parameter i.e. Grashof number (Gr) primary velocity is decelerated in the lower channel half ($-1 < \eta < 0$) whereas it is strongly accelerated in theupper channel half ($0 < \eta < 1$); the converse response is computed for the secondary flow.
- With increasing ωT values (and therefore with progression of time) there is a strongacceleration in the primary flow, whereas there secondary flow is generally retarded i.e.greater backflow.
- With a rise in magnetic field inclination (θ) the primary flow is accelerated (since hydromagnetic drag is reduced) whereas the backflow is generally decelerated i.e.increasing secondary back flow.

References

[1] Elco, R.A., Hughes, W.F. and Young, F.J.(1962). Theoretical analysis of the radial field vortex magneto-gas dynamic generator, *Zeitschrift fiir Angewandte Mathematic and Physik (ZAMP)*, ***13***, *1-13.*

[2] Katsurai, M.(1972). Studies on the MHD rotating machine, *Electrical Engineering in Japan*, ***92***, *31-43.*

[3] Ibanez,G., Cuevas,S.and Lopez de Haro,M. (2002). Optimization analysis of an alternate magnetohydrodynamic generator, *Energy Conversion and Management*, ***43***, *1757-1771.*

[4] Takhar, H.S.,Ram,P.C.and Singh,S.S. (1993). Unsteady MHD flow of adusty viscous liquid in a rotating channel with hall current, *Int. J. Energy Research*, ***17***, *69-74.*

[5] Seth,G.S., Ansari,M.S. and Nandkeolyar,R. (2010) Unsteady hydromagnetic Couette flow within porous plates in a rotating system, *Adv. Appl.Math.Mech*, ***2***, *286-302.*

[6] Hayat,T., Khan,S.B. and Khan,M. (2007). The influence of hall current on the rotating oscillating flows of an Oldroyd-B fluid in a porous medium, *Nonlinear Dynamics*, ***47***, *353-362.*

[7] Zueco, J. and Bég, O. Anwar (2010). Network numerical analysis of hydromagnetic squeeze film flow dynamics between two parallel rotating disks with

induced magnetic field effects, *Tribology International*, **43**, 532-543.

[8] Ghosh, S.K. and P.K. Bhattacharjee (2000). Magnetohydrodynamic convection flow in a rotating channel, *Archives of Mechanics*, **52**, 303-318.

[9] Ghosh, S.K. and P.K. Bhattacharjee (2000). Hall effects on steady hydromagnetic flow in a rotating channel in the presence of an inclined magnetic field, Czech. *J. Physics, 50,759-767*.

*[10]*Rawat, S., R. Bhargava, R., Renu Bhargava and O. Anwar Bég (2009). Transient magneto-micropolar free convection heat and mass transfer through a non-Darcy porous medium channel with variable thermal conductivity and heat source effects, *Proc. IMechE Part C- J.*

*[11]*Bhargava,R.,R.Sharma and O.Anwar Beg, (2009). Oscillatory chemically reacting MHD free convection heat and mass transfer in a porous medium with Soret and Dufour effects finite element modeling, *Int. J. Applied Mathematics and Mechanics**, 5,6**, 15-37*.

*[12]*Hayat,T., Hutter,K., Nadeem, S. and Asghar,S. (2004). Unsteady hydromagnetic rotating flow of a conducting second grade fluid, *Zeitschrift fiir Angewandte Mathematik und Ptysik (ZAMP), **55**, 626-641*.

*[13]*Hughes,W. and J.Young (1966). The Electro-Magneto-Dynamics of Fluids, *John Wiley, New York.*

*[14]*Meyer,R.C. (1958) .On reducing aerodynamic heat transfer rates by magnetohydrodynamic techniques, *J. Aerospace Sci, **25**, 561-566*.

*[15]*Mazumdar, B.S.(1977). Effect of wall conductances on hydromagnetic flow and heat transfer in a rotating channel, *Acta Mechanica*, ***28***, *85-99.*

*[16]*Mazumdar, B.S., Gupta, A.S. and Datta, N. (1976). Hall effects on combined free and forced convective hydromagnetic flow through a channel, *Int, J. Engineering Science, **14**, 285-292.*

*[17]*Bég, O. Anwar, J. Zueco and L. M. López-Ochoa (2011). Network numerical analysis of optically-thick hydromagnetic slip flow from a porous spinning disk with radiation flux, variable thermophysical properties and surface injection effects, *Chemical Engineering Communications**,*** **198**, 360-384.

*[18]*Bég, O. Anwar, S.K. Ghosh and T. A. Bég (2011). *Applied Magneto-Fluid Dynamics: Modelling and Computation*, 463 pages, Lambert Academic Publishing, Saarbrucken, Germany .**ISBN 978-3-8465-0865-7.**

*[19]*Vogin, C and Alemany, A. (2007). Analysis of the flow in a thermo-acoustic MHD generator with conducting walls, *Eur. J. Mechanics - B/Fluids*, **26,** 479-493.